Available online at www.sciencedirect.com
SCIENCE DIRECT
Polymer 47 (2006) 922–930
polymer
www.elsevier.com/locate/polymer

Morphology and thermal stabilization mechanism of LLDPE/MMT and LLDPE/LDH nanocomposites

Longzhen Qiu, Wei Chen, Baojun Qu *

State Key Laboratory of Fire Science and Department of Polymer Science and Engineering, University of Science and Technology of China, Hefei, Anhui 230026, China

Received 26 July 2005; received in revised form 31 October 2005; accepted 7 December 2005
Available online 28 December 2005

Abstract

The morphology and thermal stabilization mechanism of polymeric nanocomposites prepared by solution intercalation of linear low density polyethylene (LLDPE) with montmorillonite (MMT), MgAl layered double hydroxide (LDH), and ZnAl LDH have been studied by X-ray diffraction (XRD), transmission electron microscopy (TEM), dynamic Fourier transform infrared (FTIR) spectroscopy, and thermogravimetric analysis (TGA). Both LLDPE/MMT and LLDPE/MgAl LDH nanocomposites exhibit mixed intercalated–exfoliated structures, whereas the LLDPE/ZnAl LDH nanocomposites exhibit completely exfoliated structures because the ZnAl LDH layers can be easily broken during the refluxing process. All nanocomposites show significantly enhanced thermal stability compared with virgin LLDPE due to the increases of the effective activation energy (E_α) during degradation process. However, LDHs nanocomposites show much higher thermal degradation temperatures than MMT nanocomposites with the same filler content because they have much higher E_α than MMT nanocomposites at the early degradation stage. The data of real time FTIR spectroscopy and morphological evolution reveal a catalytic dehydrogenation effect presents in MMT nanocomposites, which may decrease the E_α of degradation and thermal stability of MMT nanocomposites.

Keywords: Layered double hydroxide; Nanocomposite; Thermal stabilization mechanism

1. Introduction

Polymer/layered inorganic nanocomposites formed by implanting layered inorganics into polymer matrix have been recognized as one of the most promising materials because of their excellent physicochemical properties, such as enhanced mechanical properties [1–3], thermal stability [4,5], gas impermeability [6,7], and flame retardance [8–10]. For instance, even when the clay content is as low as 0.1% in a polystyrene/layered silicate nanocomposite, the initial decomposition temperature can be increased by 40 °C and the peak heat release rate decreased by 40% compared with virgin PS [10].

The layered materials involved in this field mainly include silicates, manganese oxides, molybdenum sulfide, titanates, layered phosphates, and layered double hydroxides (LDHs). Up to now, the most common layered material is the smectite group mineral such as montmorillonite (MMT), which belongs to the general family of 2:1 layered silicates. The crystal structure of MMT consists of 1-nm thin layers with a central octahedral sheet of alumina fused between two external silica tetrahedral sheets (the oxygens from the octahedral sheet also belong to the silica tetrahedral). Isomorphic substitution of Mg^{2+} or Fe^{2+} for Al^{3+} within layers generates negative charges that are counterbalanced by Na^+ ions in the interlayers. Many preparation methods for polymer/MMT nanocomposites have been developed [11–13], such as in situ polymerization of pre-intercalated monomers, solution intercalation, melt intercalation, and template synthesis. Two classes of nanomorphologies are observed in nanocomposites: one is intercalated-type structures, in which the polymer chains are intercalated in the gallery space between the layers; the other is exfoliated-type structures, in which the delaminated layers are individually dispersed in a continuous polymer matrix.

In contrast to MMT, LDHs are host–guest materials consisting of positively charged brucite-like layers due to partial substitution of the framework divalent cations with trivalent cations. Additional charge is counterbalanced by the anions presented in the gallery spaces between the inorganic sheets. The general composition of LDHs can be presented as

* Corresponding author. Tel./fax: +86 551 360 7245.
E-mail address: qubj@ustc.edu.cn (B. Qu).

0032-3861/$ - see front matter © 2005 Elsevier Ltd. All rights reserved.
doi:10.1016/j.polymer.2005.12.017

$[M^{2+}_{1-x}M^{3+}_{x}(OH)_2]^{x+}A^{n-}_{x/n}\cdot mH_2O$, where M^{2+} and M^{3+} are divalent and trivalent metal cations, such as Mg^{2+}, Al^{3+}, respectively, A is an anion, such as Cl^-, CO_3^{2-}, SO_4^{2-} and NO^-. Because of their highly tunable properties, LDHs are considered as a new emerging class of the most favorable layered crystals for the preparation of multifunctional polymer/layered crystal nanocomposites [14]. A series of polymeric anions and water soluble polymers [15–22] have been used to prepare intercalated polymer/LDHs nanocomposites by ion-exchange reactions, in situ polymerization of pre-intercalated monomers, or co-precipitation method from the solution containing the desired polymer as a co-solute template. However, few studies were reported on the preparation of exfoliated polymer/LDH nanocomposites because of the strong interlayer electrostatic interaction, small gallery space, and hydrophilic property of LDH. O'Leary and co-workers [23] have reported that the delamination of dodecyl sulfate modified MgAl LDH in polar acrylate monomers with the help of high shearing and subsequent polymerization of the monomers containing the LDH dispersion gave exfoliated polyacrylates/LDH nanocomposites. Hsueh and Chen [24–26] have obtained the polyimide/LDH, epoxy/LDH, and PMMA/LDHs nanocomposites from the amino benzoate-intercalated, amino laurate-intercalated and 10-undecenoate-intecalated MgAl LDH, respectively. Cost and co-workers [27] also tried to prepare low-density polyethylene/LDH nanocomposites by melt-intercalation technique, but the XRD and TEM results showed that the LDH particles were not exfoliated in polymer matrix. Recently, our laboratory has developed a solution intercalation method which can obtain the polyethylene-*g*-maleic anhydride/MgAl LDH [28], low-density polyethylene/ZnAl LDH (LLDPE/ZnAl LDH) [29,30], and polystyrene/ZnAl LDH [31] exfoliated nanocomposites. Most of the mentioned-above polymer/LDH nanocomposites show significantly enhanced thermal stability.

Although the improved thermal stability of polymer/layered inorganics nanocomposites has been reported extensively, the mechanism of such a remarkable effect is not yet well understood. The most common explanation suggests that the enhanced thermal stability and fire resistant properties are derived from the mass and heat transfer barrier caused by a carbonaceous-silicate char on the surface of the polymer melt [4,5,8–10]. However, recent studies also suggest that the effect may be associated with a chemical interaction between the polymer matrix and the clay layer surface during thermal degradation and combustion processes. In the work of Zanetti et al. [32] a catalytic effect of the nanodispersed clay layers was found to be effective in promoting char-forming reaction in PP/MMT and EVA/MMT [5,9] nanocomposites. Zhu et al. [33] reported that the structural iron in clays could act as radical traps to prevent degradation. Even the organic modifiers played an important role during degradation [34,35]. Considering the results obtained from magnesium hydroxides, the nanocomposites based on polymer interleaved LDHs are reasonably considered to provide a higher thermal stability and flame resistance than silicates. However, to our knowledge, the systematical comparison of nanocomposites based on LDHs and silicates has never been investigated. In the present paper, we have studied systematically the characteristics of morphological structures and thermal behaviors of LLDPE/MMT, LLDPE/MgAl LDH, and LLDPE/ZnAl LDH nanocomposites prepared by solution intercalation. In order to better understand the enhanced thermal stabilization mechanism, dynamic FTIR and isoconversional kinetic analysis have been used to observe the structural changes and the activation energy during thermo-oxidative degradation.

2. Experimental

2.1. Materials

LLDPE (DFDC-7050) with a melting flow index of 2.0 g per 10 min and a number average molecular weight of 32,000 g mol^{-1} was supplied by Zhongyuan Petrochemical Company, China. $AlCl_3\cdot 6H_2O$, $ZnCl_2$, and ethanol (analytical pure grade) were supplied by Shanghai Zhenxing Chemicals No. 1 Plant. $MgCl_2\cdot 6H_2O$, sodium dodecyl sulfate (SDS), NaOH, and xylene (analytical pure grade) were obtained from China Medicine (Group) Shanghai Chemical Reagent Corporation. The organophilic montmorillonite (OMT) was provided by Ke Yan Company (HeFei, China). OMT was prepared from MMT by ion exchange reaction using hexadecyl trimethyl ammonium bromide (C16) in water. All these commercial chemicals were used as received without further purification.

2.2. Preparation of samples

The dodecyl sulfate modified LDH [LDH(DS)] was prepared by anion exchange method. First, the LDH precursors intercalated Cl^- [LDH(Cl)] were prepared by co-precipitation of 0.75 M $M^{2+}Cl_2$ and 0.25 M $M^{3+}Cl_3$ (where M^{2+}–M^{3+} is Mg–Al or Zn–Al) under flowing N_2 gas with vigorous stirring. The solution was adjusted to a constant pH value, in which the pH value is 10.0 for MgAl LDH and 8.0 for ZnAl LDH, by dropwise addition of 1.0 M NaOH solution. After aged in mother liquid at 60 °C for 24 h, the precipitation was washed and dried. Secondly, 1.0 g LDH(Cl) was dispersed in 100 mL 0.1 M SDS at 60 °C for 3 days, and yielded LDH(DS).

The LLDPE/clay nanocomposites (named as clay NC*x*, where *x* refers to the weight percent of clay in the nanocomposites) were prepared by solution intercalation method. A desired amount of organo-clay [OMT, Mg_3Al(DS), and Zn_3Al(DS)] was firstly refluxed in 100 mL xylene for 12 h under flowing N_2 gas at 140 °C. Then 2.0 g LLDPE was added into the suspension. After stirred for 6 h, the mixture was poured into 300 mL ethanol for rapid precipitation. The precipitate was filtered and dried at 100 °C under vacuum for 2 days.

2.3. Characterization

The X-ray diffraction (XRD) patterns were collected on a Rigaku D/Max-rA rotating anode X-ray diffractometer equipped with a Cu Kα tube and Ni filter ($\lambda = 0.1542$ nm).

The transmission electron microscopy (TEM) images were obtained on a Hitachi H-800 transmission electron microanalyzer with an accelerate voltage of 200 kV and camera length of 0.8 m. The samples were ultramicrotomed with a diamond knife on an LKB Pyramitome to give 100-nm thick slices. The slices were transferred from water to a 200-mesh Cu grid. The dynamic Fourier transfer infrared (FTIR) spectra were recorded using a Nicolet MAGNA-IR 750 Spectrometer equipped with a heating device having a temperature controller. The film samples of virgin LLDPE or nanocomposites were placed in a ventilated oven kept at 400 °C with temperature fluctuation of ±1 °C for dynamically measuring the FTIR spectra in situ during the thermo-oxidative degradation. The FTIR software was used to measure the FTIR peak intensity in order to compare the degradation rate of different materials. The relative concentration of alkyl group can be calculated by the intensity ratio of related peak height to the maximum height of 2923 cm^{-1} peak at the thermo-oxidative degradation time. Repeated experiments showed that there was no real difference for a small change of sample thickness in measuring the relative peak intensity. To investigate the morphologic evolution during thermo-oxidative degradation, a series of samples with dimension of 10×10×0.5 mm^3 were thermo-degraded in a ventilated oven kept at 400 °C with temperature fluctuation of ±1 °C for different times and recorded by a digital camera. The thermogravimetric analysis (TGA) was performed on a Shimadzu TGA-50H thermoanalyzer. In each case, about 5 mg sample was performed under an air flow rate of 6×10^{-5} m^3 min^{-1} at a scan rate of 10 °C min^{-1} from room temperature to 700 °C. For kinetic analysis of the thermo-oxidative degradation, TGA experiments of some samples were performed at four different heating rates, such as 10, 20, 30, and 40 °C min^{-1}.

2.4. Kinetic analysis

The thermal degradation kinetic parameters of LLDPE and its nanocomposites were derived based on the non-isothermal technique. In thermogravimetric analysis (TGA) curves, the conversion factor α is defined as

$$\alpha = \frac{W_0 - W_t}{W_0 - W_f} \tag{1}$$

where W_0, W_t, and W_f are the sample weights at the initial, t, and final time, respectively. The differential degradation kinetic equation can be simply expressed as

$$\frac{d\alpha}{dt} = A\, e^{-E/RT} f(\alpha) \tag{2}$$

where A is a pre-exponential factor of Arrhenius type rate constant, E is the activation energy, R is the gas constant (J mol^{-1} K), T is the temperature, and $f(\alpha)$ is a function depending on the actual reaction mechanism. Flynn and Wall have reported that the activation energy of a thermal decomposition process can be determined directly from a series of TGA curves obtained at different heating rates [36]. The Flynn–Wall method can give the E_α at a constant α by the following equation

$$\frac{-E_\alpha}{R} = \frac{1}{z}\frac{d(\ln \beta)}{d(1/T)} \tag{3}$$

where β is the heating rate (K min^{-1}), E_α is the apparent activation energy (J mol^{-1}), z is a constant of 1.05 [36–38].

3. Results and discussion

3.1. Morphology of nanocomposites

Fig. 1 shows changes of XRD patterns with the different contents of MMT, MgAl LDH, and ZnAl LDH in the LLDPE

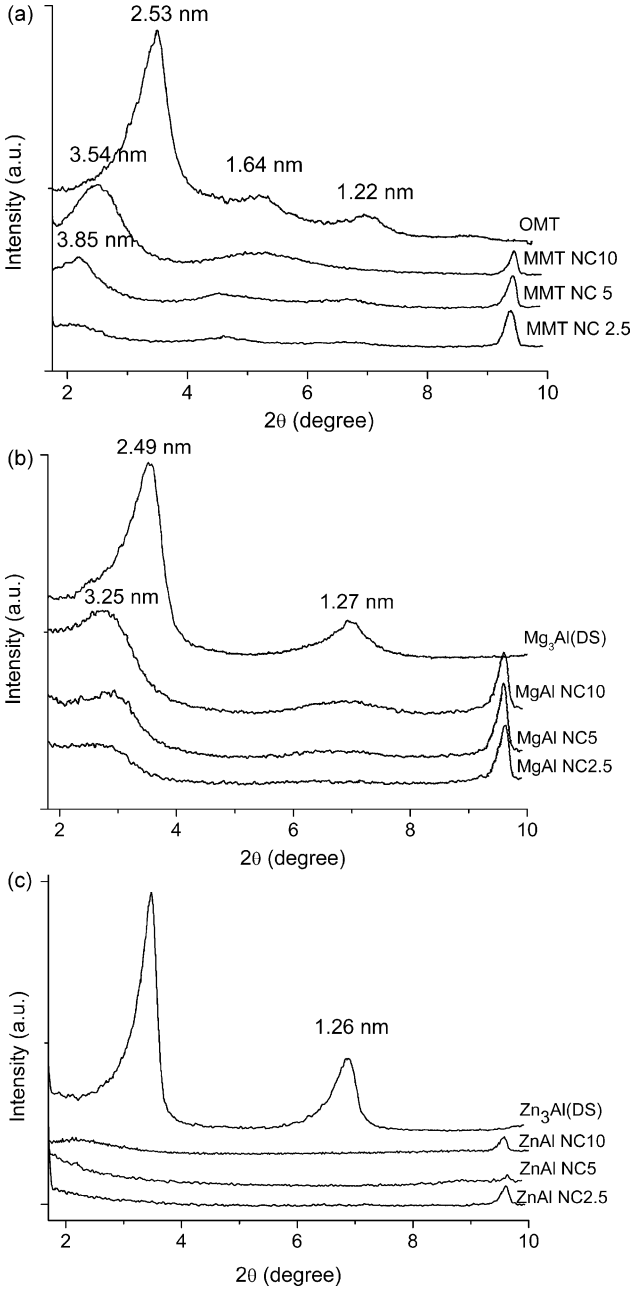

Fig. 1. Changes of XRD patterns with different contents of MMT (a), MgAl LDH (b), and ZnAl LDH (c) in the LLDPE nanocomposites.

nanocomposites. It can be seen from Fig. 1a and b that the basal spaces of MMT NC10 and MgAl NC10 nanocomposites increases to 3.54 nm from 2.53 nm of the original OMT and to 3.25 nm from 2.49 nm of the original Mg_3Al(DS), respectively. These results suggest that the PE molecular chains have intercalated into the MMT and MgAl LDH galleries. The basal spaces turn to lower angle and become broader and weaker with the decrease of the OMT and Mg_3Al(DS) content indicating the equilibrium between exfoliation and intercalation structures in the LLDPE/MMT and LLDPE/MgAl LDH nanocomposites has been driven toward exfoliation.

For Zn_3Al(DS), the diffraction peak associated with the 001 reflection of Zn_3Al(DS) component disappears completely in all the LLDPE/ZnAl LDH nanocomposites as the loading of Zn_3Al(DS) changes from 2.5 to 10 wt% (Fig. 2c). This gives a positive evidence that the ZnAl layers have been completely exfoliated in the LLDPE matrix.

The TEM images of MMT NC10, MgAl NC10, and ZnAl NC10 samples with two kinds of scale magnification are shown in Figs. 2–4, respectively. It can be seen from Fig. 2 that the MMT NC10 is mainly comprised of 10–50 nearly parallel silicate layers with about 5–10 nm interlayer spacing. The interlayer spacing is much larger than the original 1.53 nm of OMT, which gives direct evidence that the LLDPE molecules have intercalated into the OMT galleries. In addition to the intercalated structures, some exfoliated layers can also been found on the edges of the primary dispersed particles. The thickness and the lateral size of the single MMT layers can be measured as being about 1 and 150–300 nm, respectively.

The TEM images for MgAl NC10 sample (Fig. 3) also show mixed intercalated–exfoliated structures. The lateral size of the single MgAl layers can be estimated as 30–150 nm, much smaller than that of MMT.

However, the TEM images of ZnAl NC10 sample (Fig. 4) are quite different from those of MMT NC10 and MgAl NC10 samples. Compared with the face-to-fact orientated structures of OMT and Mg_3Al(DS) layers, the exfoliated Zn_3Al(DS) layers are dispersed disorderly in the LLDPE matrix. It is worth noting that a large number of small parts with a dimension of

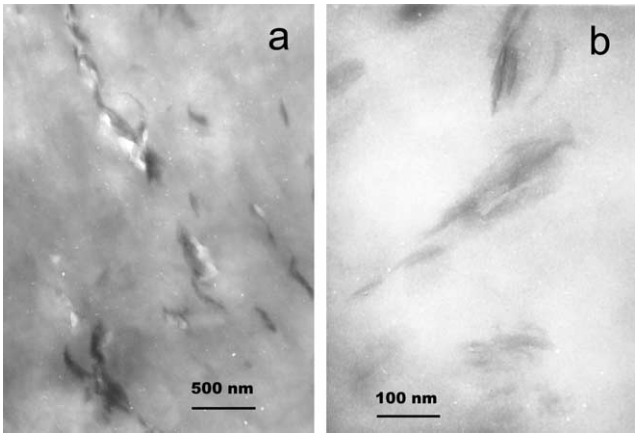

Fig. 3. TEM images of MgAl NC10 sample at (a) low and (b) high magnifications.

10–20 nm appear in the ZnAl NC10 sample, which are caused by the break of ZnAl layers when they were refluxed in xylene, as reported in our early work [30,31]. The layer-broken process may destroy the ordered crystal structure and facilitate the penetration of polymer into the center of Zn_3Al(DS) particles, and thus lead to the exfoliated structures.

The above morphologies observed by TEM are in good agreement with the XRD results. So it can be confirmed that the LLDPE/MMT and LLDPE/MgAl nanocomposites with the filler content lower than 10 wt% are the mixed intercalated–exfoliated structures whereas the LLDPE/ZnAl nanocomposites are the exfoliated structures.

3.2. Thermal stability of nanocomposites

Fig. 5 shows the TGA profiles of virgin LLDPE and its nanocomposites with different contents of MMT, MgAl LDH, and ZnAl LDH. It shows that the thermal stability of the nanocomposites is enhanced compared with that of the virgin LLDPE, which can be ascribed to the hindered effect of LDH layers on the diffusion of oxygen and volatile products throughout the composite materials. However, these

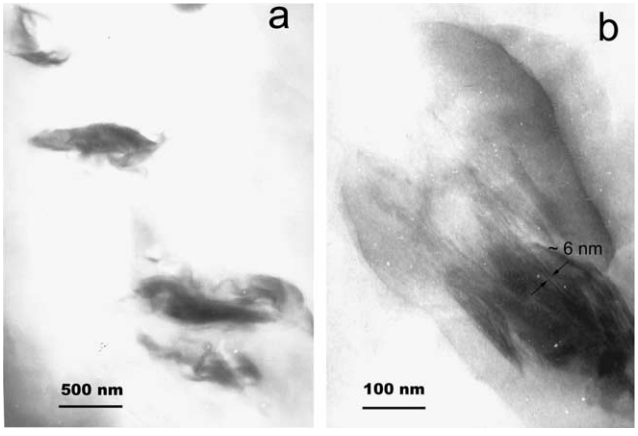

Fig. 2. TEM images of MMT NC10 sample at (a) low and (b) high magnifications.

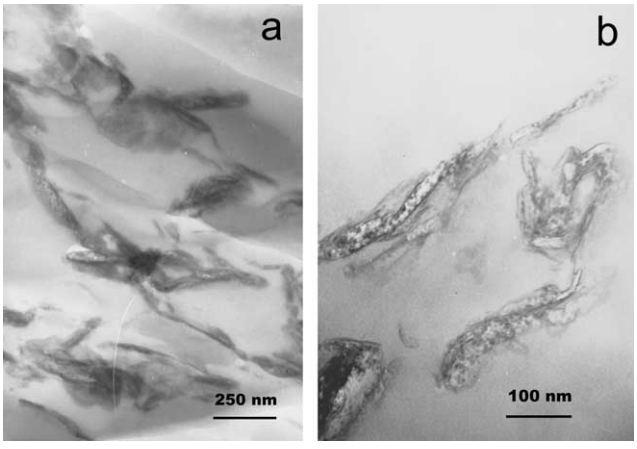

Fig. 4. TEM images of ZnAl NC10 sample at (a) low and (b) high magnifications.

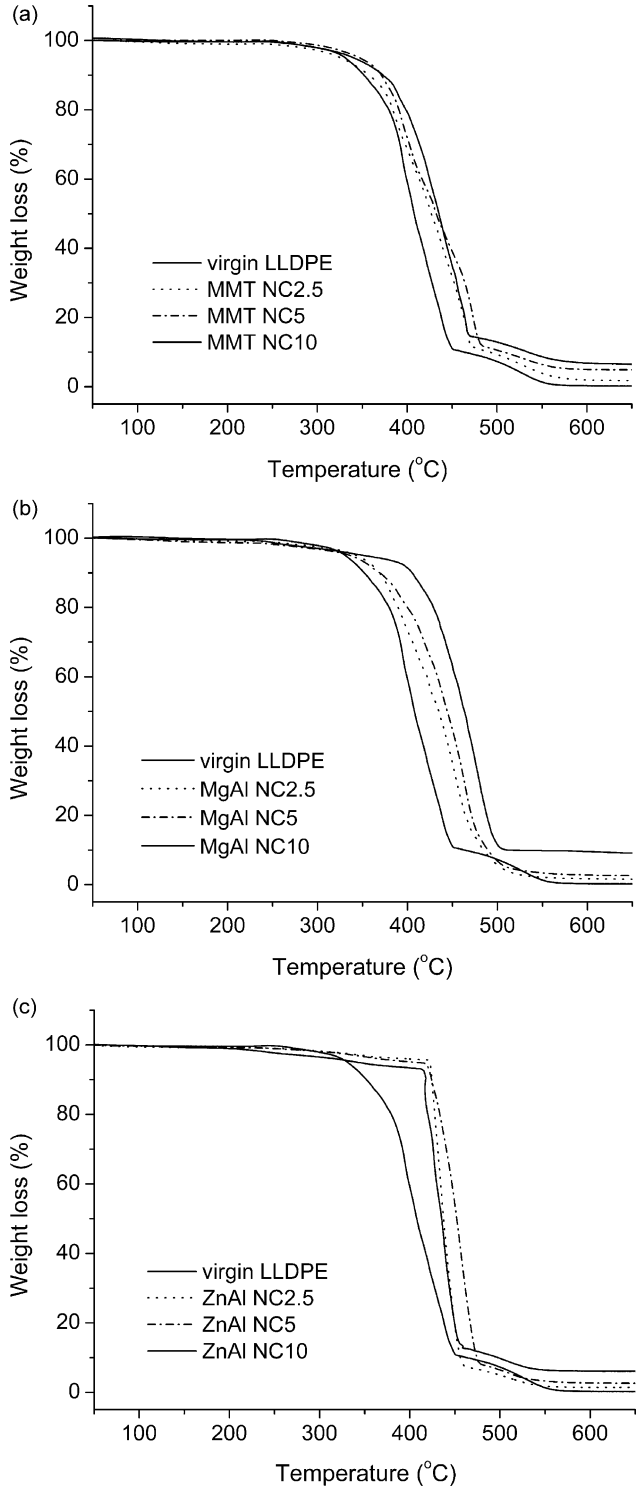

Fig. 5. Change of TGA profiles with different contents of MMT (a), MgAl LDH (b), and ZnAl LDH (c) in the LLDPE nanocomposites.

enhancements are quite different in the above three kind of nanocomposites. The changes of the temperature points at 20 wt% mass loss ($T_{0.2}$) with the contents of clay in the MMT, MgAl LDH, and ZnAl LDH nanocomposites are shown in Fig. 6. It can be seen that the $T_{0.2}$ values for the LLDPE/MMT and LLDPE/MgAl LDH samples increase gradually to 398.6 and 428.6 °C, respectively, with increasing the OMT and

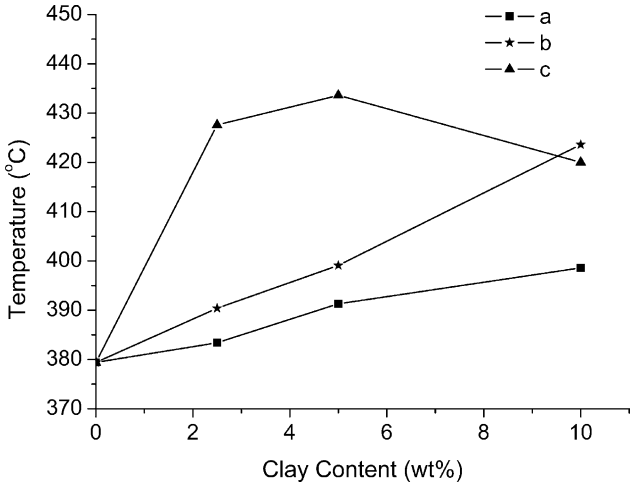

Fig. 6. The variation of the temperature of 20 wt% mass loss ($T_{0.2}$) with the content of MMT (a), MgAl LDH (b), and ZnAl LDH (c) in the LLDPE nanocomposites.

Mg_3Al(DS) contents from 0 to 10 wt%. However, LLDPE/ZnAl LDH sample with only 2.5 wt% of Zn_3Al(DS) can significantly increase the $T_{0.2}$ value to 427.6 °C. After that, it reaches the maximum of 433.6 °C when the content of Zn_3Al(DS) increases to 5 wt% and surprisingly decreases to 420.0 °C when the Zn_3Al(DS) content further increases to 10 wt%. This curious reverse trend in thermal stability has also been reported in other polymer/clay nanocomposites [39,40]. The possible reasons reported in the literature have been considered as heat source domain [39] or relative extent of exfoliation [40].

Furthermore, it can also be seen that the LLDPE/MgAl LDH and LLDPE/ZnAl LDH samples demonstrate much higher degradation temperatures than the LLDPE/MMT samples with the same clay content. When 10 wt% clay content was chosen as comparison point, the $T_{0.2}$ values of MMT NC10, MgAl NC10, and ZnAl NC10 samples are 398.6, 423.6, and 420.0 °C, respectively. Although both MMT NC10 and MgAl NC10 have mixed exfoliated–intercalated structures, $T_{0.2}$ value of the MMT NC10 sample is 25 °C lower than that of MgAl NC10.

3.3. Isoconversional kinetic analysis of thermo-oxidative degradation

The isoconversional kinetic analysis is a common method to study the kinetics of polymer degradations, which may provide information on the change of activation energy during the thermo-oxidative degradation as well as offer mechanistic clues. Fig. 7 shows the relationship of the activation energy (E_α) values calculated by the Ozawa–Flynn–Wall method with the conversion extent (α). It can be seen that the activation energies of virgin LLDPE and its nanocomposites are about 70 kJ mol^{-1} at the beginning of degradation reaction ($\alpha =$ 0.03), which indicates that the degradation of these samples is initiated by similar reactions. After that, the degradation activation energy of virgin LLDPE shows a slight increase from 62 to 111 kJ mol^{-1}, which is consistent with the

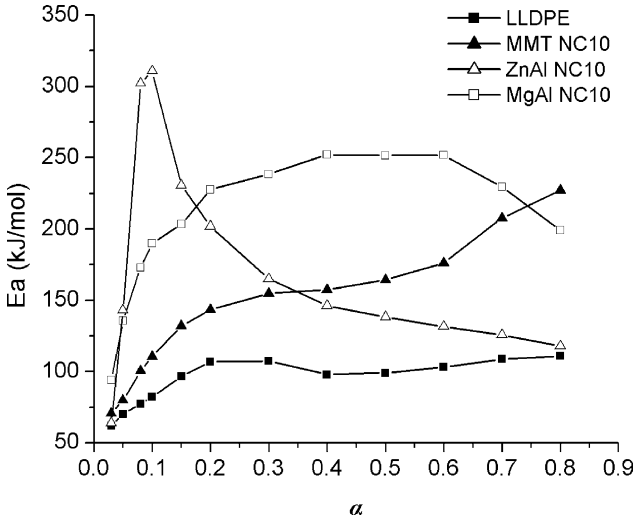

Fig. 7. Dependence of the effective activation energy on the extent of conversion for the thermo-oxidative degradation of virgin LLDPE and its nanocomposites.

activation energies (80–110 kJ mol^{-1}) of the most oxygen-initiated depolymerization. All three nanocomposites samples show higher activation energy after the initial degradation reactions. The activation energy of the MMT NC10 sample gradually increases from 60 to 150 kJ mol^{-1} during the first degradation stage ($\alpha < 0.6$), which indicates that the process kinetic is limited by peroxide radical decomposition. At the following stage ($\alpha > 0.6$), the activation energy rapidly increases to around 220 kJ mol^{-1}, which is similar to the activation energy obtained by degradation of PE under inert gas, as reported in the literature [41–43]. These observations indicate that the rate-limiting step in the thermo-oxidative degradation of MMT NC10 have changed from peroxide radical decomposition to random scission decomposition. In the case of the MgAl NC10 and ZnAl NC10 samples, the E_α values sharply increase to 227 and 310 kJ mol^{-1} at the early degradation stage ($\alpha = 0.1$–0.2), respectively, indicating the change of rate-limiting step has happened in this stage. After that, the E_α value of the MgAl NC10 sample levels off at 227–252 kJ mol^{-1} in the range of $\alpha = 0.2$–0.6 followed by a rapid decreases to 199 kJ mol^{-1} at $\alpha = 0.8$, while the E_α value of the ZnAl NC10 sample rapidly decreases to 146 kJ mol^{-1} at $\alpha = 0.4$.

Putting the above results together we may conclude that the nano-dispersed inorganic layers cause an anaerobic condition in the samples, as indicated by the change of rate-limiting step in the thermo-oxidative degradation from peroxide radical decomposition to random scission decomposition. These results are well consistent with the barrier model mechanism, which suggests that the inorganic layers play a barrier effect on the diffusion of oxygen from gas phase into the nanocomposites.

It should be noticed that the changes of rate-limiting step happened at very different stages in those samples. Considering the TGA results which show much higher degradation temperatures in the LLDPE/MgAl LDH and LLDPE/ZnAl LDH samples than in the LLDPE/MMT samples with the same clay content, we wonder if there are other factors that influence the thermal stability except for the barrier effects.

3.4. Thermo-oxidative degradation behaviors of nanocomposites

In order to obtain a better insight into the thermal stabilization mechanism of the LLDPE nanocomposites, dynamic FTIR was used to observe the structural changes and identify the products formed during thermo-oxidative degradation [44–46]. Furthermore, the degradation rates of polymers can be obtained by measuring the relative intensity of the absorption peaks of polymers. Fig. 8 shows the changes of dynamic FTIR spectra with different thermo-oxidative degradation time of virgin LLDPE, MMT NC10, MgAl NC10, and ZnAl NC10 samples in the condensed phase at 400 °C. In the case of virgin LLDPE, the intensities of two peaks at 2925 and 2854 cm^{-1} assigned to the –CH_2– or –CH_3 asymmetric and symmetric stretching vibration and the two peaks at 1455 and 1346 cm^{-1} from asymmetric deformation vibration of –CH_2– and –CH_3 groups decrease rapidly with increasing thermo-oxidative degradation time. The absorption peak at 720 cm^{-1} due to the deformation vibration in –$(CH_2)_n$– ($n \geq 4$) groups disappears after 30 s pyrolysis. These results indicate that the C–H and C–C main chains of PE are broken gradually. The thermo-oxidative degradation of LLDPE leads to the formation of a broad band at 1850–1650 cm^{-1}, which suggests that the LLDPE has been oxidized to carbonyl groups. The strong absorption around 1600 cm^{-1} is assigned to the C=C stretching vibration. Table 1 lists the detailed assignments of these FTIR absorption peaks together with the corresponding literature [44–49].

The dynamic FTIR spectra of nanocomposites are very similar to that of virgin LLDPE apart from some absorption peaks of filler. It is worthy to note that two different features appear in the range of 1500–1900 and 2800–3000 cm^{-1}. Fig. 9 compares the variations of absorbance in the range from 1500 to 1900 cm^{-1} as a function of thermo-oxidative degradation time for virgin LLDPE, MMT NC10, MgAl NC10, and ZnAl NC10, respectively. It can be seen that the thermal degradation of MgAl NC10 and ZnAl NC10 mainly leads to alkenes compared with the major carbonyl products in the virgin LLDPE and MMT NC10, indicating that the MgAl NC10 and ZnAl NC10 samples have better barrier effect on oxygen.

Fig. 10 shows the changes of the relative peak intensity at 2925 cm^{-1} with the degradation time. Apparently, the decreasing rates of 2925 cm^{-1} peak intensity of the MgAl NC10 and ZnAl NC10 samples are similar and both are much slower than the virgin LLDPE, whereas the MMT NC10 sample shows a higher decreasing rate than the virgin LLDPE. It seems contrary to the TGA results which show enhanced thermal stability in all three nanocomposites. In order to explain the conflict, a digital camera was used to monitor the morphologic evolution during the thermo-oxidative degradation process.

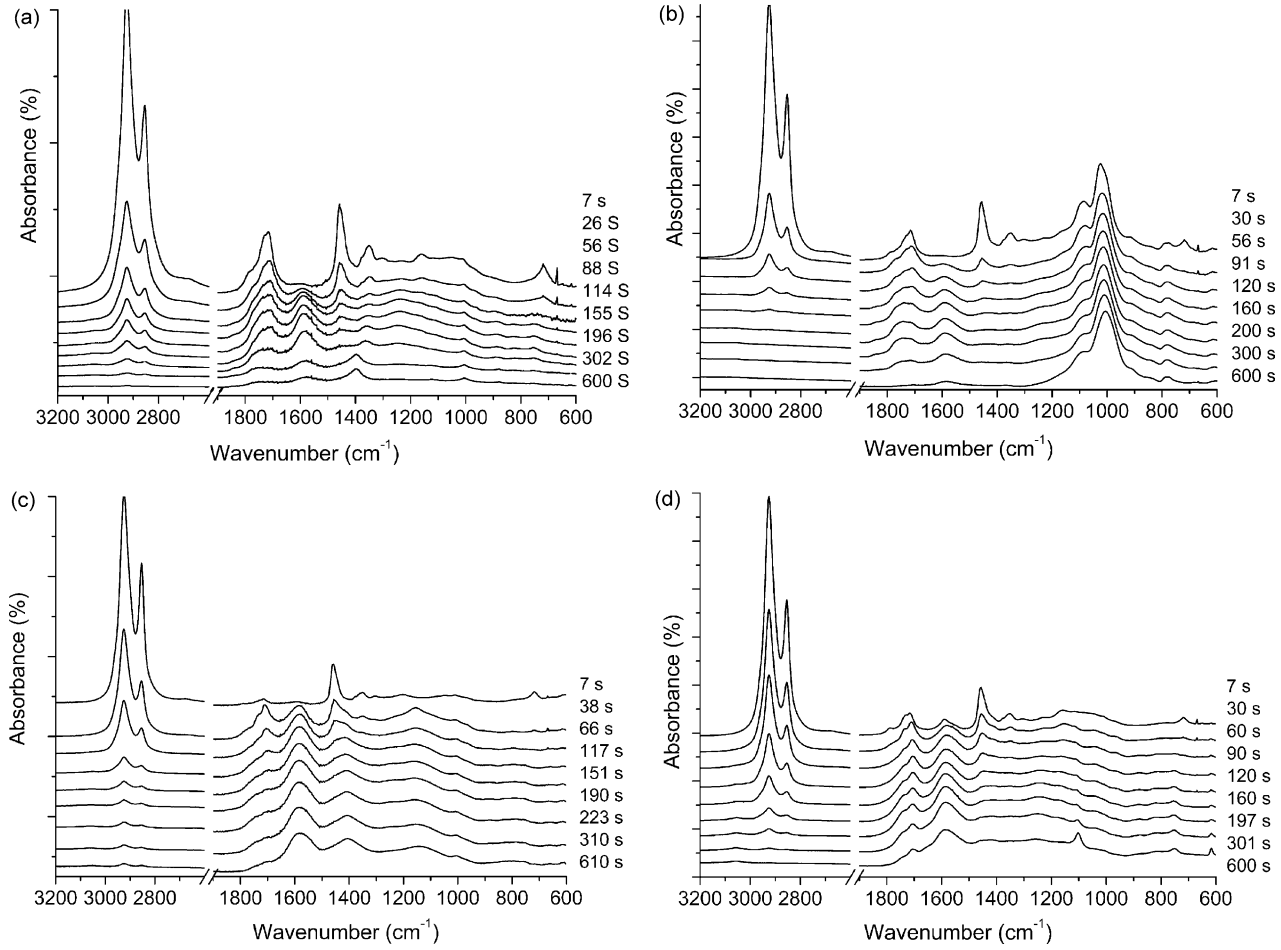

Fig. 8. Dynamic FTIR spectra with different thermo-oxidative time at 400 °C: (a) virgin LLDPE, (b) MMT NC10, (c) MgAl NC10, and (d) ZnAl NC10.

3.5. Morphologic evolutions during thermo-oxidative degradation of nanocomposites

Fig. 11 shows the morphologic evolutions of virgin LLDPE, MMT NC10, MgAl NC10, and ZnAl NC10 samples with different degradation time at 400 °C. It can be seen that the color of the virgin LLDPE samples becomes darker and darker with increasing degradation time because of the thermo-oxidation degradation of PE chains. At the same time, some volatile thermo-oxidative products were released from the sample indicated by the yellow tail around it. After 10 min degradation time, most of the virgin LLDPE samples have been degraded.

The surface of the MMT NC10 sample is much darker than the corresponding virgin LLDPE sample with the same degradation time, which indicates that a char layeres formed on the surface of the MMT NC10 samples. This result is consistent with the catalytic dehydrogenation effect observed in dynamic FTIR. The char formation plays a very important role in the improvement of thermal stability because the MMT NC10 sample with 10 min degradation time still keeps the original shape and leaves over a large amount of charred residue.

The relative light color surface indicating the dehydrogenation was hindered in the LDH nanocomposites. No volatile

Table 1
Assignment of the dynamic FTIR spectra obtained from the thermo-oxidative of LLDPE and its nanocomposites in the condensed phase

Wavenumber (cm^{-1})	Assignment	Reference
3060	ν(C–H) in alkene	[45]
2925	$\nu(CH_2)_a$	[44]
2854	$\nu(CH_2)_s$	[44]
1840	ν(C=O) in cyclic anhydride	[47]
1785	ν(C=O) in peracids	[43]
1763	ν(C=O) in peresters	[43]
1741	ν(C=O) in ester	[45,46]
1730	ν(C=O) in aldehyde	[48]
1718	ν(C=O) in ketone	[45,46]
1713	ν(C=O) in carboxylic acid	[45–47]
1698	ν(C=O) in α–β unsaturated ketone	[45]
1590	ν(C=C)	[45]
1461	$\delta(CH_2)_a$	[44]
1356	$\delta(CH_2)_s$	[44]
1160	ν(C–O) in ester	[44,45]
1100	ν(Si–O)	[45]
1010	ν(Si–O)	[45]
720	$\gamma(CH_2)$	[45]

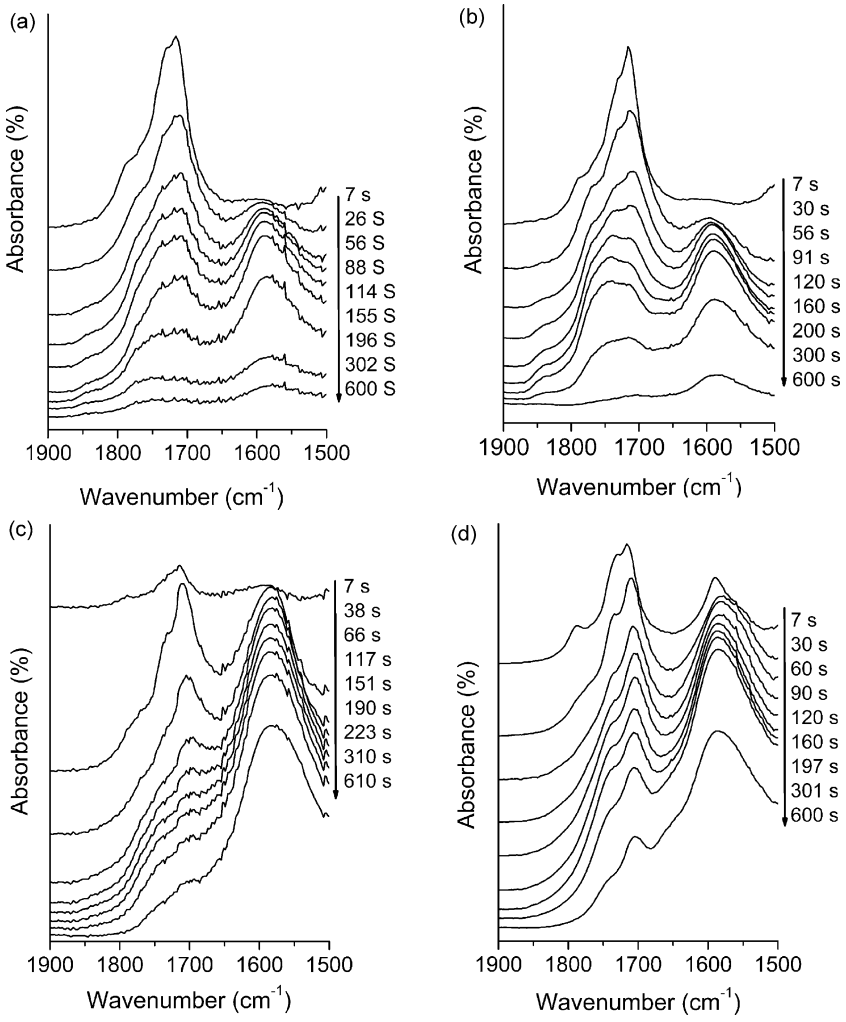

Fig. 9. Changes of dynamic FTIR spectra of (a) virgin LLDPE, (b) MMT NC10, (c) MgAl NC10, and (d) ZnAl NC10 in the range of 1500–1900 cm^{-1}.

products can be observed from MgAl NC10 and ZnAl NC10 samples when the degradation time increased to 10 min suggesting they have higher thermal stability than virgin LLDPE and MMT NC10. Another feature in these samples is that a large amount of bubbles (as marked with arrow in Fig. 11) formed during degradation, which may be caused by the accumulation of volatile degradation products. At the later stage of degradation, these bubbles burst out and destroy the compact surface of the samples. This may be the main reason for the rapid decrease of activation energy in MgAl NC10 and ZnAl NC10, as shown in Fig. 7.

As a result of above discussion, we can see that the enhanced thermal stability mechanisms of LLDPE/MMT and LLDPE/LDH nanocomposites are very different. The former have lower effective activation energy at the early stages of thermal degradation because the presence of MMT layers can catalyze the dehydrogenation of LLDPE molecule. After that, ceramic-carbonaceous layers formed on the surface of the material might act as an excellent mass transport barrier and created an anaerobic inner. However, the LLDPE/LDH nanocomposites have very high effective activation energy at the early stages of thermal degradation. During this process, the LDH layers may function by providing barrier layers on the surface of samples and by releasing aqueous vapour that may absorb heat, exclude oxygen, and dilute flammable gases. When the degradation temperature further increases, a large

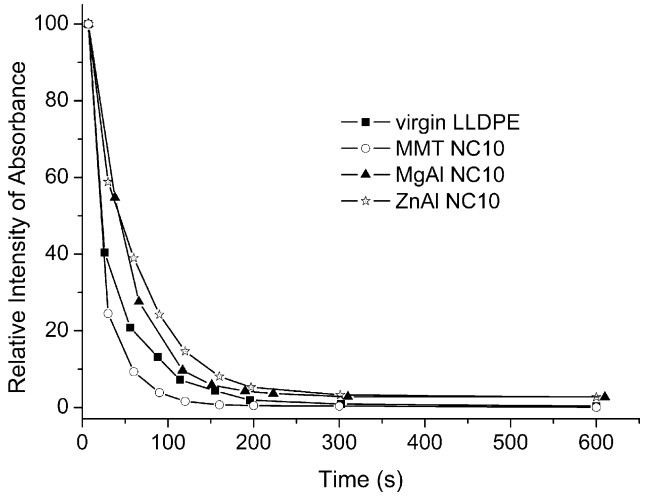

Fig. 10. Relative peak intensities of absorbance at 2925 cm^{-1} assigned to the $-CH_2-$ or $-CH_3$ asymmetric vibration in the LLDPE and its nanocomposites.

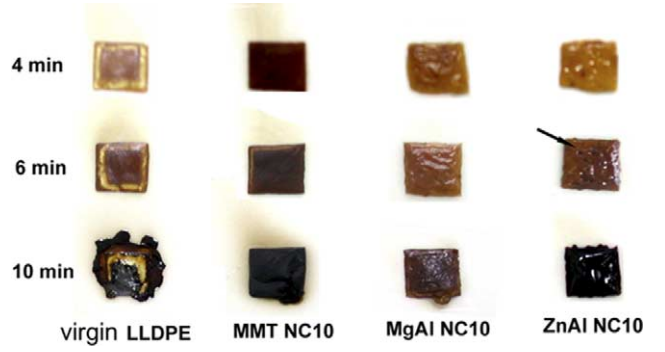

Fig. 11. Morphologic evolutions of virgin LLDPE, MMT NC10, MgAl NC10, and ZnAl NC10 samples with different thermo-oxidative time at 400 °C observed by the digital camera.

amount of volatile products generated at the first degradation stage burst out from inner of samples and destroy the barrier layers.

4. Conclusion

LLDPE/MMT, LLDPE/MgAl LDH, and LLDPE/ZnAl LDH nanocomposites can be prepared by a solution intercalation method. The XRD and TEM data show that the LLDPE/MMT and LLDPE/MgAl nanocomposites are mixed intercalated–exfoliated structures, while the LLDPE/ZnAl nanocomposites are exfoliated structures with clay content less than 10 wt% because the ZnAl LDH layers can be easily broken in the refluxing process. All the nanocomposites show significantly enhanced thermal stability compared with the virgin LLDPE. It has been found from the TGA data that the exfoliated structures show more effective enhancement of the thermal stability than intercalated structures. However, the thermal property of nanocomposites is determined not only by the morphological structures but also by the chemical components of clays. The LDHs nanocomposites show much higher thermal stability than the MMT nanocomposites when they have the same filler content and similar structures. The data of dynamic FTIR spectroscopy, morphological evolution, and isoconversional kinetic analysis reveal the two different mechanisms of enhanced thermal stability in the LLDPE/MMT and LLDPE/LDHs nanocomposites. The former is mainly based on the protective charred layers formed by the MMT catalysis dehydrogenation of PE molecules, whereas the latter is based on the barrier effect of LDH layers with very high activation energy, which prevents the diffusion of oxygen from gas phase into the polymer nanocomposites and thus not only protects the C–C main chain from the thermal degradation but also hinders the dehydrogenation process of PE molecules.

Acknowledgements

This work was supported by the National Natural Science Foundation of China, No. 50373039 and the China NKBRSF project, NO. 2001 CB409600.

References

[1] Tyan HL, Liu YC, Wei KH. Chem Mater 1999;11:1942.
[2] Tyan HL, Leu CM, Wei KH. Chem Mater 2001;13:222.
[3] Choi YS, Wang KH, Xu M, Chung IJ. Chem Mater 2002;14:2936.
[4] Blumstein A. J Polym Sci A 1965;3:2665.
[5] Zanetti M, Camino G, Thomann R. Polymer 2001;42:4501.
[6] Yano K, Usuki A, Olada A, Kurauchi T, Kamigaito O. J Polym Sci, Part A: Polym Chem 1993;31:2493.
[7] Sinha Ray S, Yamada K, Okamoto M, Ogamin A, Ueda K. Chem Mater 2003;15:1456.
[8] Gilman JW, Jackson CL, Morgan AB, Harris R, Manias E, Giannelis EP, et al. Chem Mater 2000;12:1866.
[9] Zanneti M, Kashiwangi T, Falqui L, Camino G. Chem Mater 2002;14:881.
[10] Zhu J, Wilkie CA. Polym Int 2000;49:1158.
[11] Lagaly G. Appl Clay Sci 1999;15:1.
[12] Alexandre M, Dubios P. Mater Sci Eng R 2000;28:1 [references therein].
[13] Sinha Ray S, Okamoto M. Prog Polym Sci 2003;28:1539.
[14] Leroux F, Basse JP. Chem Mater 2001;13:3507.
[15] Vaysse C, Guerlou-Demourgues L, Duguet E, Delmas C. Inorg Chem 2003;42:4559.
[16] Whilton NT, Vickers PJ, Mann S. J Mater Chem 1997;7(8):1623.
[17] Moujahid EM, Besse JP, Leroux F. J Mater Chem 2003;13:258.
[18] Oriakhi CO, Farr IV, Lerner MM. J Mater Chem 1996;6:103.
[19] Yang QZ, Sun DJ, Zhang CG, Wang XJ, Zhao WA. Langmuir 2003;19:5570.
[20] Messersmith PB, Stupp SI. J Mater Res 1992;7:2599.
[21] Messersmith PB, Stupp SI. Chem Mater 1995;7:454.
[22] Challier T, Slade RCT. J Mater Chem 1994;4:367.
[23] O'Leary S, O'Hare D, Seeley G. Chem Commun 2002;1506.
[24] Hsueh HB, Chen CY. Polymer 2003;44:1151.
[25] Hsueh HB, Chen CY. Polymer 2003;44:5275.
[26] Wang GA, Wang CC, Chen CY. Polymer 2005;46:5065.
[27] Cost FR, Abdel-Goad M, Wagenknecht U, Heinrich G. Polymer 2005;46:4447.
[28] Chen W, Qu BJ. Chem Mater 2003;15:3208.
[29] Chen W, Feng L, Qu BJ. Chem Mater 2004;16:368.
[30] Chen W, Qu BJ. J Mater Chem 2004;14:1705.
[31] Qiu LZ, Chen W, Qu BJ. Polym Degrad Stab 2005;87:433.
[32] Zanetti M, Camino G, Reichert P, Mulhaupt R. Macromol Rapid Commun 2001;22:176.
[33] Zhu J, Uhl FM, Morgan AB, Wilkie CA. Chem Mater 2001;13:4649.
[34] Zhu J, Morgan AB, Lamelas FJ, Wilkie CA. Chem Mater 2001;13:3774.
[35] Su S, Wikie CA. Polym Degrad Stab 2004;83:347.
[36] Flynn JH, Wall LA. J Polym Sci, Polym Lett 1966;4:323.
[37] Wang ZZ, Wu GS, Hu Y, Ding Y, Hu KL, Fan WC. Polym Degrad Stab 2002;77:427.
[38] Ballice L. Fuel 2001;80:1923.
[39] Lim ST, Hyun YH, Choi HJ. Chem Mater 2002;14:1839.
[40] Paul MA, Alexandre M, Degée P, Henrist C, Rulmont A, Dubois P. Polymer 2003;44:443.
[41] Peterson JD, Vyazovkin S, Wight CA. Macromol Chem Phys 2001;202:775.
[42] Westerhout RWJ, Balk RHP, Meijer R, Kuipers JAM, van Swaaij WPM. Ind Eng Chem Res 1997;36:3360.
[43] Bockhorn H, Hornung A, Hornung U. J Anal Appl Pyrolysis 1999;50:77.
[44] Luongo JP. J Polym Sci 1960;42:139.
[45] Xie RC, Qu BJ, Hu KL. Polym Degrad Stab 2001;72:313.
[46] Zanetti M, Bracco P, Costa L. Polym Degrad Stab 2004;85:657.
[47] Costa L, Luda MP, Trossarelli L. Polym Degrad Stab 1997;58:41.
[48] Morlat S, Mailhot B, Gonzalez D, Gardette J. Chem Mater 2004;16:377.
[49] Wu QH, Qu BJ, Xu YH, Wu Q. Polym Degrad Stab 2000;68:97.